

Article type : MS - Regular Manuscript

**Carbon allocation to major metabolites in illuminated leaves is not just proportional to photosynthesis when gaseous conditions (CO<sub>2</sub> and O<sub>2</sub>) vary**

Cyril Abadie, Camille Bathellier and Guillaume Tcherkez

Research School of Biology, College of Science, Australian National University, 2601 Canberra, ACT  
Australia

Author for correspondence:

*Guillaume Tcherkez*

*Tel: +61 6125 0381*

*Email: guillaume.tcherkez@anu.edu.au*

Received: *6 October 2017*

Accepted: *29 November 2017*

This is the author manuscript accepted for publication and has undergone full peer review but has not been through the copyediting, typesetting, pagination and proofreading process, which may lead to differences between this version and the [Version of Record](#). Please cite this article as [doi: 10.1111/nph.14984](https://doi.org/10.1111/nph.14984)

This article is protected by copyright. All rights reserved

## Summary

- In gas-exchange experiments, manipulating CO<sub>2</sub> and O<sub>2</sub> is commonly used to change the balance between carboxylation and oxygenation. Downstream metabolism (utilization of photosynthetic and photorespiratory products) may also be affected by gaseous conditions but this is not well documented.
- Here, we took advantage of sunflower as a model species, which accumulates chlorogenate in addition to sugars and amino acids (glutamate, alanine, glycine and serine). We performed isotopic labelling with <sup>13</sup>CO<sub>2</sub> under different CO<sub>2</sub>/O<sub>2</sub> conditions, and determined <sup>13</sup>C-contents to compute <sup>13</sup>C-allocation patterns and build-up rates.
- The <sup>13</sup>C-content in major metabolites was not found to be a constant proportion of net fixed carbon but rather, changed dramatically with CO<sub>2</sub> and O<sub>2</sub>. Alanine typically accumulated at low O<sub>2</sub> (hypoxic response) while photorespiratory intermediates accumulated under ambient conditions and at high photorespiration, glycerate accumulation exceeding serine and glycine build-up. Chlorogenate synthesis was relatively more important under normal conditions and at high CO<sub>2</sub> and its synthesis was driven by phosphoenolpyruvate *de novo* synthesis.
- These findings demonstrate that carbon allocation to metabolites other than photosynthetic end products is affected by gaseous conditions and therefore the photosynthetic yield of net nitrogen assimilation varies, being minimal at high CO<sub>2</sub> and maximal at high O<sub>2</sub>.

**Key words:** carbon allocation, labelling, nitrogen assimilation, NMR, photorespiration, photosynthesis.

## Introduction

Photosynthetic CO<sub>2</sub> assimilation and photorespiration rely on metabolic cycles in which 3-phosphoglycerate (PGA) is used to synthesize triose phosphates and regenerate ribulose-1,5-bisphosphate (RuBP), and 2-phosphoglycolate is recycled back to PGA. RuBP consumption and regeneration are balanced so that phosphorylated metabolic pools are regulated and photosynthesis operates in the steady-state (von Caemmerer & Farquhar, 1981; Sage *et al.*, 1988). Similarly, 2-phosphoglycolate conversion to photorespiratory intermediates glycine, serine and glycerate, and then to PGA should in principle be quantitative so that no

progressive imbalance in the photorespiratory cycle arises. However, it has been recently shown that the effective stoichiometric coefficient between CO<sub>2</sub> evolution by photorespiratory metabolism and O<sub>2</sub> consumption by RuBP oxygenation deviates very slightly from 2, so that glycine tends to accumulate in the illuminated leaf (Abadie *et al.*, 2016a). Photosynthetic end products such as sucrose also tend to accumulate in the light, reflecting the utilization of triose phosphates synthesized by the Calvin cycle (Huber, 1989). Therefore, both leaf carbohydrate and amino acid content change with the carboxylation-to-oxygenation ratio. However, the current knowledge of general reorchestration of leaf metabolism beyond direct photosynthetic and photorespiratory products when photosynthesis or photorespiration rates (CO<sub>2</sub>/O<sub>2</sub> ratio) vary is still fragmentary. In addition, it is common practice to assume that the amount of carbon directed to downstream components (or end products) is a constant proportion of net photosynthetic input (Penning De Vries, 1983; Hilbert & Reynolds, 1991; Dewar *et al.*, 1998).

To our knowledge, a precise flux-analysis through sucrose and hexose phosphates pools under varying CO<sub>2</sub>/O<sub>2</sub> ratio has never been undertaken. Sucrose synthesis and translocation seems to be scaled to photosynthesis, regardless of the origin of changes in photosynthetic activity (light or CO<sub>2</sub>) (Servaites & Geiger, 1974), except at low CO<sub>2</sub> where carbon allocation to sucrose proportionally increases a lot (Sharkey *et al.*, 1985). Also, photosynthesis in 100% O<sub>2</sub> has been found to cause a proportionally lower carbon allocation (i.e., a lower fraction of net fixed carbon) to sugars (Maleszewski & Lewanty, 1972) but 2% O<sub>2</sub> causes little changes in carbon allocation to neutral sugars as compared to 21% O<sub>2</sub> (Nakamura *et al.*, 1997). Leaf sucrose content is determined by enzymes of sugar metabolism such as invertase and a synthesis-degradation futile cycle (Geiger, 1979; Huber, 1989; Geigenberger & Stitt, 1991), both of which possibly changing with the metabolic context. For example, decreased expression of sucrose phosphate synthase (SPS) and cytosolic fructose-1,6-bisphosphatase (cFBPase) by antisense technology does not lead to the same effects, with typically much less accumulation of phosphorylated intermediates upon SPS activity reduction compared to cFBPase activity (Strand *et al.*, 2000). This has been suggested to be caused by the decrease in pyrophosphate content (PPi) and a shift of the UDP-glucose/hexose phosphate ratio, thereby favouring sucrose synthesis when SPS is down-regulated. Presumably, when photosynthesis varies with the CO<sub>2</sub>/O<sub>2</sub> ratio, changes in metabolite pool sizes including inorganic phosphate (Pi) and fructose-2,6-bisphosphate (effectors acting on sucrose synthesis) (Stitt, 1990) could modulate the flux of net sucrose synthesis.

In general, there seems to be a relationship between sucrose and amino acid production and export by illuminated leaves so that the synthesis of N-containing compounds are expected to be scaled to photosynthesis rate (Foyer *et al.*, 2000). However, using isotopic labelling with  $^{13}\text{C}$ -citrate,  $^{13}\text{CO}_2$  or  $^{15}\text{N}$ -nitrate and NMR analyses, it has been shown that nitrogen (N) assimilation *per se* is affected by  $\text{CO}_2$  and  $\text{O}_2$  mole fraction, so that *de novo* glutamate synthesis tends to increase as photorespiration increases (Gauthier *et al.*, 2010; Tcherkez *et al.*, 2012; Abadie *et al.*, 2017b). Similarly, increased photorespiration rates have been shown to be associated with higher electron consumption for N assimilation (Bloom *et al.*, 2002, 2014; Rachmilevitch *et al.*, 2004). It has also been demonstrated that protein synthesis is stimulated by light (as opposed to the dark) while the phosphorylation of cytosolic translation initiation factors is affected by  $\text{CO}_2$  mole fraction (Piques *et al.*, 2009; Boex-Fontvieille *et al.*, 2013). Biosynthesis of cell constituents like cellulose also responds to photosynthesis, with more cellulose synthesis at high  $\text{CO}_2$  (but representing less when expressed as a ratio of net photosynthesis) (Boex-Fontvieille *et al.*, 2014). Finally, monitoring the tricarboxylic acid pathway (TCAP) using  $^{13}\text{C}$ -pyruvate labelling has shown that respiratory metabolism responds to  $\text{CO}_2$  and  $\text{O}_2$ , so that the flux associated with decarboxylations increases with photorespiration (Tcherkez *et al.*, 2008).

Taken as a whole, carbon fluxes do not seem to be strictly scaled to photosynthesis, due to metabolic interactions between photorespiration, N assimilation and other pathways (such interactions are further discussed in Hodges *et al.*, 2016). Furthermore, although many fluxes mentioned above (non-quantitativity of photorespiratory conversions, TCAP, and *de novo* glutamate synthesis) are numerically small (compared to photosynthesis or photorespiration), the potential impact of their variation on leaf metabolism may be considerable. In fact, even an imbalance as small as  $0.1 \mu\text{mol m}^{-2} \text{s}^{-1}$  in glycine recycling in photorespiration generates an excess demand for N assimilation of *c.*  $5 \text{mmol m}^{-2} \text{d}^{-1}$ , representing nearly 10% of total leaf N content. Similarly, the consumption of PGA at a rate of  $0.1 \mu\text{mol m}^{-2} \text{s}^{-1}$  by chloroplastic anabolism (for example, to synthesize phosphoenolpyruvate, PEP) represents a net consumption of *c.*  $2 \text{mmol RuBP m}^{-2} \text{d}^{-1}$ , that is, much more than total RuBP content of most leaves ( $\approx 80 \mu\text{mol m}^{-2}$  in sunflower, Jacob & Lawlor 1992). Therefore, even very small changes in metabolism downstream of carboxylation or oxygenation *per se* can have pervading consequences on RuBP regeneration, N assimilation and anabolic pathways.

Despite this importance, there is currently no precise quantitative data on carbon allocation patterns (including build-up rates of photorespiratory intermediates) when photosynthesis varies due to CO<sub>2</sub> and O<sub>2</sub> mole fraction. Here, we used steady-state <sup>13</sup>CO<sub>2</sub> labelling on leaves and <sup>13</sup>C-NMR analyses to trace precisely the fate of fixed carbon in metabolic pools and examine their changes with CO<sub>2</sub> and O<sub>2</sub> mole fraction. NMR analyses are less sensitive than mass spectrometry but are highly quantitative, thereby allowing us to: (1) focus on leaf metabolites that are quantitatively important for carbon metabolism ('major' metabolites) and (2) determine absolute <sup>13</sup>C amounts (e.g., in mmol m<sup>-2</sup>). Also, it reveals information on intramolecular isotopic pattern and thus the potential utilization of distinct metabolic pools for different C-atom positions of molecules. We have previously taken advantage of NMR analysis and mass-balance calculations to trace the origin of carbon atoms used for *de novo* glutamate synthesis (Abadie *et al.*, 2017b). In the present paper, major metabolites were followed so as to calculate their apparent <sup>13</sup>C-allocation from net fixed <sup>13</sup>CO<sub>2</sub>. We took advantage of sunflower as a model species, which accumulates chlorogenate in leaves (Steck, 1968; Lehman & Rice, 1972) in addition to primary metabolites derived from sugar metabolism, photorespiration, or the TCAP (Fig. 1). Chlorogenate is a phenylpropanoid synthesized from erythrose-4-phosphate (E4P) and PEP (Supporting Information Figs S1, S2). Also, sunflower is a broadly used oil-producing crop with a relatively low carbon use efficiency (Connor & Sadras, 1992; Albrizio & Steduto, 2003) and therefore carbon allocation and utilization is a question of prime importance in this species. We used six different CO<sub>2</sub>/O<sub>2</sub> conditions, to answer the following questions: (1) Is carbon allocation to sucrose, fructose and glucose pools sensitive to CO<sub>2</sub> and O<sub>2</sub> conditions? (2) Do apparent fluxes to amino acids and chlorogenate accumulation represent a constant proportion of net photosynthesis? (3) Does the resulting metabolic demand in N assimilation vary with net photosynthesis?

## Materials and Methods

### Plant material

Sunflower seeds (*Helianthus annuus* L., var. XRQ) were sown in potting mix and after 14 d, plantlets were transferred to 15-l pots. Plants were grown in the glasshouse under 24 : 18°C, 60 : 55% relative humidity, 16 h : 8 h, day : night photoperiod, with natural light supplemented by Lucagrow 400 W sodium lamps (JB Lighting, Cheltenham, Australia).

Plants were watered every 2 d supplemented once a week with 1.5 g l<sup>-1</sup> nutrient solution Peters<sup>®</sup> Professional Pot Plant Special (Everris, the Netherlands) with a N/P<sub>2</sub>O<sub>5</sub>/K<sub>2</sub>O composition of 15/11/29 (and a nitrogen balance nitrate/ammonium/urea of 8.6/2.0/4.4) and trace elements.

### Gas exchange and sampling

Gas-exchange under controlled CO<sub>2</sub>/O<sub>2</sub> conditions was performed in chambers coupled to the Licor 6400-XT (Licor Biosciences, USA), with soft walls that could be cut very quickly and thus allowed instant sampling by liquid nitrogen spraying, as described previously (Tcherkez *et al.*, 2012). The leaf chamber was adapted to individual leaves with a surface area of *c.* 100 cm<sup>2</sup>. Gas-exchange conditions were 80% relative humidity and 21–23°C air temperature. Isotopic labelling was performed using <sup>13</sup>CO<sub>2</sub> (Sigma-Aldrich, 99% <sup>13</sup>C) for 2 h after having reached steady photosynthesis using ordinary CO<sub>2</sub> (natural abundance) for *c.* 60 min. For all CO<sub>2</sub>/O<sub>2</sub> conditions, two series of experiments were done: with <sup>13</sup>CO<sub>2</sub>, and with natural CO<sub>2</sub>. Performing experiments with natural CO<sub>2</sub> was strictly required for %<sup>13</sup>C calculations using NMR data. Six CO<sub>2</sub>/O<sub>2</sub> conditions were used here (%-μmol mol<sup>-1</sup>, ordered by increasing carboxylation-to-oxygenation ratio): 100-380, 21-140, 21-380, 21-800, 2-380, 0-380. In figures, the *x*-axis shows these conditions in that order. Gaseous conditions used in the present study are summarized in Table S1.

### Extraction and NMR analysis

Samples (100 cm<sup>2</sup>, i.e. *c.* 2 g FW) were extracted with perchloric acid in liquid nitrogen as previously described in (Aubert *et al.*, 1994). Briefly, the sample was ground with liquid nitrogen with 900 μl perchloric acid 70% and 500 μl of maleate solution 0.5 M (i.e. a total of 125 μmol per sample, used as an internal standard). The fine powder was poured in a 50 ml centrifuge tube and then 10 ml MilliQ water were added. After centrifugation (15,000 *g*, 15 min), the pellet was re-extracted with 3 ml perchloric acid 2% and centrifuged. The two supernatants were combined, pH-adjusted to 5 with potassium bicarbonate and frozen-dried. Then the sample was re-suspended in 1 ml water, pH-adjusted to 7 with KOH and centrifuged. 550 μl of supernatant were collected, 50 μl D<sub>2</sub>O were added and the sample was poured in a 5-mm NMR tube (Z107373, Bruker Biospin). Samples were analyzed with NMR

spectrometer Advance 700 Mz (Bruker Biospin). NMR analyzes were performed at 298 K (25°C) without tube spinning, using proton-decoupled (decoupling sequence waltz16) carbon pulse program (zgif) with 90° pulses for  $^{13}\text{C}$  of 10  $\mu\text{s}$  at 50 W, 0.9 s acquisition time, 65 k size of FID, and a relaxation delay (D1) of 1.2 s. To get a good signal-to-noise ratio, 20,000 scans were done, representing *c.* 12 h analysis per sample. Since the response of individual peaks at different chemical shifts is not perfectly quantitative under such acquisition conditions (short D1), signals were corrected using calibrating samples with known concentrations of standard metabolites (Glu, Asp, Ala and threonine). In practice, correction factors were within 0.9-1.1 and thus were of little importance. NMR data presented in the paper are mean $\pm$ SD of  $n = 3$  replicates.

### *LC-MS*

Liquid chromatography was performed using a ZIC®-HILIC column (3.5  $\mu\text{m}$ , 200 Å, 150 x 2.1 mm, Merck SeQuant®) coupled with a ZIC®-HILIC column guard (20 x 2.1 mm, Merck SeQuant®) at 30°C oven temperature, with a LC system UHPLC<sup>+</sup> Ultimate 3000 (Dionex-Thermo Scientific, Hemel Hempstead, UK). Aliquots from the NMR extraction were diluted 10 times in water/acetonitrile (v:v, 50:50) and an internal standard (trifluoromethyl phenylalanine, TFMP) was added to monitor the signal response of the LC-MS. For quantification, calibration curves with a mixture of standard amino acids (including TFMP) were done before and after sample batches. The sample-tray was set at 4°C (constant temperature). Injection volume was 1  $\mu\text{L}$  and elution was done at a flow rate of 0.3  $\text{ml min}^{-1}$  with a binary gradient. Mobile phase A was acetonitrile/water (v:v, 25:75) and mobile phase B was acetonitrile/water (v:v, 95:5) both with ammonium acetate (5 mM). The gradient applied was 72% B at 0 min down to 36% B at 13 min and maintained for 2 min, and then back to 72% B at 16 min (total run time of 21 min). For MS analysis, an Orbitrap Q Exactive Plus (Thermo Fisher Scientific) with a HESI-II probe was operated in positive polarity using the full MS scan mode with the following settings: source voltage 3,500 V, resolution 70,000, AGC target  $1 \cdot 10^6$ , mass scan range 60-600 m/z, sheath gas 40, auxiliary gas 10, sweep gas 1.5, probe temperature 300°C, capillary temperature 250°C and S-lens RF level 50. Mass calibration was performed with the LTQ-ESI positive ion calibration solution (Pierce®, Thermo Fisher Scientific) immediately before each analysis batch. The software Xcalibur was used to handle LC-MS data. LC-MS data presented in the paper are mean $\pm$ SD of  $n = 6$  replicates.

## Calculations

The percentage in  $^{13}\text{C}$  was calculated as the ratio of the NMR signal of the C-atom position obtained upon  $^{13}\text{C}$ -labelling ( $^{13}\text{S}$ ) to that obtained with ordinary  $\text{CO}_2$  (natural abundance) ( $^{12}\text{S}$ ):  $\%^{13}\text{C} = ^{13}\text{S}/^{12}\text{S} \times 1.1/99 \times 100$  where 99 and 1.1 stand for the isotopic enrichment in inlet  $\text{CO}_2$ . Calculation of accumulation fluxes for glycine, serine and glycerate were performed using mass-balance equations and convergence of the solution of the differential equation describing  $^{13}\text{C}$  pools (see Fig. S3 for calculation details). The rate of oxygenation was estimated as  $v_o = 2v_c C^*/c_i$  where  $C^*$  is the  $c_i$ -based  $\text{CO}_2$  compensation point in the absence of day respiration ( $40 \mu\text{mol mol}^{-1}$ ), and  $v_c = (A + R_d)/(1 - C^*/c_i)$  where  $R_d$  is day respiration (here  $0.5 \mu\text{mol m}^{-2} \text{s}^{-1}$ ), with  $\Gamma^*$  and  $R_d$  obtained using the Laisk method (for a recent description of this method, see Tcherkez *et al.*, 2017). Note that  $v_o$  is not used to compute  $^{13}\text{C}$  allocation fluxes and is not critical at all. A proper value of  $v_o$  (with  $\Gamma^*$  and  $c_c$  determined using internal conductance) would only change the scale in Fig. S12.

## Results

### Major metabolites in leaf extracts

The  $^{13}\text{C}$ -NMR spectrum in sunflower leaf extract is shown in Fig. 2. Even at  $^{13}\text{C}$  natural abundance (in blue), there were visible peaks associated with fumarate (C-atoms 2 + 3), sugars and chlorogenate, demonstrating their relatively high amount in leaves. Chlorogenate was formally identified using  $^{13}\text{C}$  chemical shifts values and comparison with an authentic standard (Fig. S4; Table S2). Upon  $^{13}\text{C}$  labelling, detected  $^{13}\text{C}$  was mostly found in sugars but also in chlorogenate, serine, glycine, glutamate and alanine (red spectrum in Fig. 2). Some COOH groups were also labelled but the spectral resolution (peak width) was too poor to identify them precisely. Considering  $^{13}\text{C}$ -metabolites observed here, these COOH groups mostly corresponded to malate, glycine, serine, and chlorogenate. All visible C-atoms in chlorogenate appeared to be labelled (black arrowheads in Fig. 2 and magnification in Fig. S5) showing  $^{13}\text{C}$  labelling in precursors E4P and PEP. The amount of these two compounds was nevertheless too small to be visible by  $^{13}\text{C}$  NMR here (typically  $< 10 \mu\text{mol m}^{-2}$ ). It is worth noting that two metabolites appeared to be insensitive to  $^{13}\text{C}$  labelling (i.e., with a very slow turn-over rate): fumarate and a metabolite with a peak at 53.4 ppm (likely corresponding

to magnesium phytate or a  $\text{CH}_x\text{-NH}_2$  group of a metabolite of the betaine family; letter 'b' in Fig. 2).

### Photosynthesis and sugar metabolism

As expected, net photosynthesis (denoted as  $A$ ) increased as the  $\text{CO}_2$ -to- $\text{O}_2$  ratio increased. However, at 0%  $\text{O}_2$   $A$  was  $1 \mu\text{mol m}^{-2} \text{s}^{-1}$  lower than at 2%  $\text{O}_2$  showing the impact of hypoxic conditions on photosynthetic metabolism (Fig. 3a). Total assimilated carbon during experimental time (2 h with  $^{13}\text{CO}_2$ ) increased as the  $\text{CO}_2$ -to- $\text{O}_2$  ratio increased and the most abundant  $^{13}\text{C}$  pool was found to be sucrose (Fig. 3b). Fructose, glucose and other metabolites represented a minor proportion of leaf  $^{13}\text{C}$ .  $^{13}\text{C}$  non visible in perchloric extracts (mostly representing exported sugars and starch, and marginally other fractions such as proteins or  $\text{CO}_2$  lost by day respiration) always represented *c.* 30% of net assimilated carbon, except at low  $\text{CO}_2$  ( $140 \mu\text{mol mol}^{-1}$ ) where is represented nearly 50%. When plotted against net assimilated carbon, the  $^{13}\text{C}$  amount found in leaf fructose and glucose appeared to be nearly linear while that found in sucrose was hyperbolic suggesting a saturating effect at high photosynthesis (Fig. 3c). In particular, the  $^{13}\text{C}$  amount in sucrose at high  $\text{CO}_2$  ( $800 \mu\text{mol mol}^{-1}$ ) typically was low (arrow in Fig. 3c), suggesting a change in carbon redistribution under such conditions. The %  $^{13}\text{C}$  in sucrose also decreased at high photosynthesis (Fig. 3d) showing a decline in turn-over. This effect was visible in all C-atom positions of sucrose (Fig. S6a,b). Interestingly, the average positional %  $^{13}\text{C}$  across symmetrical sucrose positions (both fructosyl and glucosyl moieties) had a flat profile, with no significant differences between C-atom positions (Fig. S6, inset). This indicates that (1) source triose phosphates used to synthesize hexoses and sucrose likely had a homogeneous intramolecular  $^{13}\text{C}$ -distribution, and (2) differences between positions in sucrose were due to  $^{13}\text{C}$  redistribution by sugar metabolism, such as triose phosphate isomerization and aldolization, and isomerization between glucose-6-phosphate and fructose-6-phosphate.

The %  $^{13}\text{C}$  in glucose plateaued and was always relatively low (a few %) (Fig. 3e), simply reflecting the isotopic dilution by the naturally very large glucose content in sunflower leaves (data not shown). The %  $^{13}\text{C}$  in fructose showed a considerable increase at high  $\text{CO}_2$  (Fig. 3f). Expected %  $^{13}\text{C}$  values in sugars were calculated from  $^{13}\text{C}$  allocation (obtained from integrals in sugars on NMR spectrum after  $^{13}\text{C}$  labelling, expressed as a % of total spectrum integral) and the total content (from NMR spectrum at natural abundance). The comparison of

expected %  $^{13}\text{C}$  with observed values (Fig. S7) shows that at high  $\text{CO}_2$ , sucrose was less  $^{13}\text{C}$ -enriched than expected and this  $^{13}\text{C}$ -depletion matched nearly perfectly the higher-than-expected  $^{13}\text{C}$ -enrichment in fructose. This demonstrates that at high  $\text{CO}_2$ , changes in active/inactive pool distribution occurred so that more  $^{13}\text{C}$ -sucrose was cleaved to generate free fructose.

### $^{13}\text{C}$ -labelling pattern of chlorogenate and its precursors

The %  $^{13}\text{C}$  in chlorogenate was always  $< 7\%$  but varied with atmospheric  $\text{CO}_2$  and  $\text{O}_2$  mole fraction. Maximal  $^{13}\text{C}$ -enrichment in chlorogenate was not observed at high photosynthesis (low oxygen) but under ambient  $\text{CO}_2$  and  $\text{O}_2$  ('usual' conditions) or high  $\text{CO}_2$  (Fig. 4a). This effect was observed not only for the whole-molecule average %  $^{13}\text{C}$  (Fig. 4a) but for all C-atom positions (Fig. S8a). This suggests that the utilization of both PEP and E4P for chlorogenate synthesis was impeded by both high photorespiration (high  $\text{O}_2$  or low  $\text{CO}_2$ ) and very low oxygen. Accordingly, the total  $^{13}\text{C}$ -amount represented by accumulated chlorogenate was higher under 'usual' conditions and at high  $\text{CO}_2$  (Fig. 4b). As a result, chlorogenate was not related at all to net assimilated carbon and represented a  $^{13}\text{C}$  allocation  $< 1\%$  (Fig. 4c).

The  $^{13}\text{C}$ -enrichment in intermediates of chlorogenate synthesis, phenylalanine and quinate, was determined using LC-MS (their amount was far too low to allow analysis by NMR). Phenylalanine and quinate followed the same pattern as in chlorogenate, with maximal %  $^{13}\text{C}$  under 'usual' conditions (Fig. 4d). Despite the relatively low  $^{13}\text{C}$ -enrichment of the chlorogenate pool,  $^{13}\text{C}$ -chlorogenate molecules formed during labelling were associated with  $\{^{13}\text{C}-^{13}\text{C}\}$  coupling, showing the simultaneous labelling in adjacent C-atom positions (Fig. S5). This was also the case in phenylalanine and quinate, in which the M+9 and M+7 masses, respectively, were observed by LC-MS and increased under 21/380, 21/800 and 2/380  $\text{CO}_2/\text{O}_2$  conditions (Fig. S9a,b). This shows the simultaneous labelling of adjacent C-atom positions. However, it is worth noting that phenylalanine showed a specific enrichment in the M+3 signal (regardless of  $\text{CO}_2/\text{O}_2$  conditions) (Fig. S9a) demonstrating the addition of a  $^{13}\text{C}_3$  unit (in practice,  $^{13}\text{C}_3$ -PEP) during the synthesis of chorismate from shikimate (pathway recalled in Fig. S2).

Line-fitting NMR signal deconvolution also allowed us to determine the proportion of molecules simply, doubly or triply  $^{13}\text{C}$ -labelled at each C-atom position in chlorogenate. As

expected, there was a general increase in  $\{^{13}\text{C}-^{13}\text{C}\}$  couplings with photosynthesis, showing increased  $^{13}\text{C}$ -labelling in E4P and PEP pools as the photosynthetic input increased (Fig. S8b). However,  $\{^{13}\text{C}-^{13}\text{C}\}$  coupling was less pronounced at low oxygen, thereby following the pattern seen for  $\%^{13}\text{C}$ .

### Build-up of photorespiratory intermediates

Three photorespiratory intermediates were visible here: glycine, serine and glycerate (Fig. 1; see Fig. S10 for the NMR identification of glycerate). The  $^{13}\text{C}$ -amount (corrected for natural abundance) represented by glycerate was always larger than that in glycine and serine (Fig. 5a). In fact, glycine represented  $< 0.5 \text{ mmol } ^{13}\text{C m}^{-2}$  (that is,  $< 1\%$  of net assimilated carbon regardless of  $\text{CO}_2/\text{O}_2$  conditions). While accumulated  $^{13}\text{C}$ -glycine increased with increased photorespiration (decreased photosynthesis), the amount of  $^{13}\text{C}$ -serine was more variable, and was maximal under ‘usual’ conditions.  $^{13}\text{C}$ -glycerate represented *c.*  $2 \text{ mmol m}^{-2}$  except at low oxygen ( $< 0.5 \text{ mmol m}^{-2}$ ) and low  $\text{CO}_2$  (*c.*  $1.2 \text{ mmol m}^{-2}$ ). Total carbon flux represented by glycerate, serine or glycine accumulation (escaping from the photorespiratory cycle) was calculated taking into account isotopic dilution (see Fig. S3 for further details). For glycine and serine, calculated fluxes were based on the visible C-atom position (C-2). In fact, for glycerate, calculations yielded the same result regardless of the C-atom position used (Fig. S11) showing that there was no bias due to potential heterogeneous intramolecular  $^{13}\text{C}$ -distribution in photorespiratory intermediates. This agrees with the rather homogeneous intramolecular  $^{13}\text{C}$ -distribution in triose phosphates (see above; Fig. S6). The accumulation (build-up) flux was always very small (Fig. 5b), much  $< 0.1 \text{ } \mu\text{mol m}^{-2} \text{ s}^{-1}$  for glycine and serine. Observed fluxes were all very close to zero at low oxygen, and serine and glycerate accumulation was maximal under ‘usual’ conditions. Glycine build-up appeared to correlate to photorespiration (increased as net photosynthesis decreased) (Fig. 5a). This was consistent with the absolute total amount of glycine and serine measured by LC-MS (Fig. 5, inset), which tended to increase as photorespiration increased. That said, this effect was more pronounced for glycine than for serine, so that the glycine-to-serine ratio increased from  $\approx 0.2 \text{ mol mol}^{-1}$  at low photorespiration to  $\approx 1 \text{ mol mol}^{-1}$  at high photorespiration. The apparent difference in glycine content between high  $\text{CO}_2$  and  $100\% \text{ O}_2$  represented *c.*  $0.6 \text{ mmol m}^{-2}$ , suggesting that glycine accumulation flux due to high photorespiration was  $\leq 0.05 \text{ } \mu\text{mol m}^{-2} \text{ s}^{-1}$ , as effectively found by isotopic mass-balance (Fig. 5b). Taken as a whole, the total build-up

flux (glycerate + serine + glycine) represented a carbon flux  $\leq 0.7 \mu\text{mol C m}^{-2} \text{ s}^{-1}$  (maximal value, observed under 'usual' conditions), accounting for 1-10% of the carbon flux represented by oxygenation (Fig. S12).

### *<sup>13</sup>C-labelling in downstream metabolites (alanine, malate and glutamate)*

Alanine accumulation was visible under all conditions but was high at low oxygen, reaching nearly  $0.3 \mu\text{mol m}^{-2} \text{ s}^{-1}$  under 0% O<sub>2</sub> (Fig. 5b). Since alanine is typically accumulated under hypoxia, this suggests that illuminated leaves experienced hypoxic conditions when subjected to an atmosphere at 0 or 2% O<sub>2</sub>. Glutamate also accumulated to small amounts (Fig. 6a) at a low rate (Fig. 6b), typically  $< 0.06 \mu\text{mol m}^{-2} \text{ s}^{-1}$  regardless of gaseous conditions. However, when expressed as a proportion of net assimilation, the flux to <sup>13</sup>C-glutamate accumulation increased as photosynthesis decreased, except at 2% O<sub>2</sub> where the value was similar to that found at 21% O<sub>2</sub>  $380 \mu\text{mol mol}^{-1}$  (Fig. 6b, inset). The <sup>13</sup>C-amount in malate was calculated using the C-atom position C-3 and multiplied by 3 (assuming no heterogeneous intramolecular distribution) so that the C-4 atom position was not accounted for (it derives from bicarbonate and its isotope composition is difficult to determine). Therefore, it represented the potential flux of <sup>13</sup>C-PEP to anaplerotic activity. The resulting <sup>13</sup>C-flux was rather variable although tended to be higher at low photosynthesis and lower under 0% O<sub>2</sub> (Fig. 6b). When expressed as a proportion of net photosynthesis, it clearly increased up to 1.6% as photosynthesis decreased (Fig. 6b, inset).

## **Discussion**

Is sucrose metabolism altered at high photosynthesis (high CO<sub>2</sub> or low O<sub>2</sub>)?

Despite a general increase in total <sup>13</sup>C amount in leaf sugars as well as starch + exported carbon as photosynthesis increased with the CO<sub>2</sub>/O<sub>2</sub> ratio, the carbon allocation (in % of assimilated carbon) to leaf sugars did not remain constant (Fig. 3c). It has also been found that the metabolic commitment to starch synthesis increases at the expense of sucrose may occur during growth at high CO<sub>2</sub>, when sucrose production (or export) is altered, or under moderate phosphorus limitation (Stitt, 1991; Rao & Terry, 1995; Sun *et al.*, 2011). We previously showed a small decrease in the sucrose content at high CO<sub>2</sub> in *Arabidopsis* rosettes (Abadie *et al.*, 2016b). Here, we provide an explanation of this phenomenon whereby the flux of sucrose synthesis was redirected to fructose accumulation at high CO<sub>2</sub>. Since no concurrent increase

was seen in glucose, this suggests that sucrose was cleaved by sucrose synthase (Susy) rather than invertase, thereby generating fructose and UDP-glucose, the latter being recycled to sucrose by sucrose phosphate synthase (SPS). In *Arabidopsis*, phosphoproteomics have shown that SPS phosphorylation vary with CO<sub>2</sub>/O<sub>2</sub>, the SPS-1F isoform being preferred at low photosynthesis and SPS-4F at high photosynthetic activity (Boex-Fontvieille *et al.*, 2014; Abadie *et al.*, 2016b). Conversely, in 0% O<sub>2</sub>, there is also a decrease in carbon allocation to sucrose, likely due to the hypoxic effect. In fact, hypoxia may have impeded cytosolic ATP synthesis and thus UDP-glucose, the substrate of sucrose synthesis by SPS (Planchet *et al.*, 2017). Taken as a whole, our results suggest that a change in the balance between Susy and SPS activities may be at the origin of the observed change in sucrose turn-over when gaseous conditions vary.

#### Photorespiratory intermediates accumulation rate

The accumulation of photorespiratory intermediates is a long-standing question that recently attracted attention because of its potential impact on photosynthetic efficiency. However, the precise measurements of the rate at which photorespiratory intermediates may accumulate is still a matter of debate (for a review, see Tcherkez, 2013). Here, we find that three visible photorespiratory intermediates glycine, serine and glycerate accumulate (Fig. 5), and this agrees with our previous observation that glycine is not completely utilized by the conversion to serine (via the glycine decarboxylase serine hydroxymethyl transferase complex) so that the effective stoichiometric coefficient between oxygenation (glycine production  $v_o$ ) and CO<sub>2</sub> evolution (serine synthesis) is slightly higher than 2 (Abadie *et al.*, 2016a). The present results further provide direct evidence that serine and glycerate also accumulated and that such a build-up carbon flux was very sensitive to CO<sub>2</sub> and O<sub>2</sub> conditions. It is worth noting that the average imbalance in glycine utilization was found to be *c.* 3% (with respect to  $v_o$ ) in (Abadie *et al.*, 2016a) while here, it is found to be *c.* 0.5%. There are presently two possible explanations. First, the sunflower variety was different (XRQ here versus *Sunrich*) and the spectrum of accumulated metabolites (like serine and glycerate) differed. In another sunflower variety (*Mennonite*), using <sup>14</sup>CO<sub>2</sub> labelling Atkins & Canvin (1971) have shown that serine represented as much as 12% of leaf radioactivity while glycine and glycolate + glycerate represented only 4 and 5%, respectively. Second, despite a similar NPK

balance, fertilization conditions differed in that urea was included in the nutrient mixture used in the present study, likely leading to a difference in N utilization by metabolism.

Our direct measurement of carbon allocation using the  $^{13}\text{C}$ -labelling method shows that the accumulation rate of glycine and serine is of the same order of magnitude (*c.*  $0.05 \mu\text{mol m}^{-2} \text{s}^{-1}$ ) as N assimilation estimated concurrently using glutamate *de novo* synthesis (Fig. 6b). Leaves also contained  $^{13}\text{C}$ -labelled glycerate in amounts even larger than serine and glycine (Fig. 5). Glycerate accumulation due to photorespiration implies that some carbon atoms required for PGA and RuBP recovery are missing (i.e., photorespiratory cycle not closed). Presumably, this has to be compensated for by a lower triose phosphates utilization for starch and sucrose synthesis (Geiger & Servaites, 1994).

Chlorogenate synthesis by the shikimate pathway is impacted by gaseous conditions

Interestingly, maximal  $^{13}\text{C}$  flux values in glycerate were found to occur in ‘usual’ conditions and at high  $\text{CO}_2$ , in which chlorogenate synthesis was also maximal. Further, metabolomics have shown a covariation between quinate (intermediate of chlorogenate synthesis) and glycerate, as well as an increase in caffeate and caffeoylquinate when  $\text{CO}_2/\text{O}_2$  decreases (Abadie *et al.*, 2016a). Here, we found that quinate and phenylalanine followed the same isotopic pattern as total  $^{13}\text{C}$  in chlorogenate (Fig. 4). In other words, it seems there was a stimulation of the shikimate pathway when glycerate accumulated. Since chlorogenate requires chloroplastic metabolites as well ATP (shikimate kinase), the covariation between  $^{13}\text{C}$  contents in chlorogenate and glycerate could reflect the competition between photorespiratory recycling (glycerate kinase) and secondary metabolism for chloroplastic ATP. Alternatively, the slightly lower PGA (and thus triose phosphates) production by photorespiratory recycling could have caused a slight imbalance in transaldolase and/or transketolase activities during the Calvin cycle and thus excess E4P could have been used for chlorogenate synthesis. In fact, a slight decrease in transketolase activity in transgenic tobacco leaves has been shown to cause a significant reduction in aromatic amino acids and downstream metabolites such as phenylpropanoids (Henkes *et al.*, 2001). The relationship between chlorogenate and glycerate could also be due to compartmentalization. Glycerate is transported by an antiport protein (glycolate-glycerate translocator) of the chloroplast envelope (Pick *et al.*, 2013) but may also be translocated using an alternative, light-dependent pathway that operates in the antiporter mutant (Walker *et al.*, 2016). Thus, the efficiency of

glycerate transport might depend on gaseous conditions (but to our knowledge, this has not been documented yet).

The shikimate pathway itself could also be regulated by photosynthetic and photorespiratory conditions. For example, varying PEP production could be at the origin of the observed changes in the carbon allocation to chlorogenate. PEP can be synthesized by both chloroplastic and cytosolic metabolisms and in the latter case, PEP enters the chloroplast via the PEP/phosphate translocator (Fig. S2, and see Tzin & Galili, 2010; Tohge *et al.*, 2013). Potentially, PEP can be synthesized by (1) enolase from 2-phosphoglycerate, (2) pyruvate Pi dikinase (PPDK) from pyruvate, and (3) PEP carboxykinase from oxaloacetate. Cytosolic and plastidic glycolysis operates at light, so that PEP production by enolase does occur in illuminated leaves, and in fact antisense technology has suggested that enolase activity is critical for the shikimate pathway (Voll *et al.*, 2009). The regulation of enolase activity is not well documented (although hypoxia has been shown to increase cytosolic enolase activity in maize, Lal *et al.*, 1994). PPDK activity has been shown to increase in the light compared to the dark via phosphorylation and a nearly significant ( $P = 0.052$ )  $\text{CO}_2/\text{O}_2$  effect has been found in (Abadie *et al.*, 2016b). PEP carboxykinase is involved in gluconeogenesis and is not associated with any changes in its phosphorylation with  $\text{CO}_2/\text{O}_2$  so that its involvement in the control of PEP production is rather unlikely.

Variation in the recycling of stored metabolic pools can also influence the  $^{13}\text{C}$  build-up in chlorogenate. Here, we find that totally labelled molecules were important isotopic species in both quinate and phenylalanine (Fig. S9a,b) indicating that fully turned-over PEP and E4P chloroplastic pools have been used to synthesize new quinate and phenylalanine molecules. However, the clear appearance of the M+3 isotopic species in phenylalanine suggests that fully labelled PEP ( $^{13}\text{C}_3\text{-PEP}$ ) was combined to non-labelled shikimate by 5-*enolpyruvylshikimate-3-phosphate* (EPSP) synthase to synthesize EPSP (and then chorismate and phenylalanine). That is, 'old' (slow turned-over) shikimate (or quinate) was remobilized, and such a remobilization appeared to depend on gaseous conditions (Fig. S9, inset). At first glance, remobilization does not appear to be consistent with the concurrent synthesis of fully  $^{13}\text{C}$ -labelled quinate, phenylalanine and chlorogenate because all of the enzymatic steps up to phenylalanine are believed to take place in the same compartment (chloroplast) (Maeda & Dudareva, 2012). Thus, remobilized shikimate (or quinate) came from either the vacuole or the cytosol and entered the chloroplast; or there is a cytosolic EPSP synthase in sunflower, consuming cytoplasmic  $^{13}\text{C}_3\text{-PEP}$  (derived from triose phosphates) and remobilized, non-

labelled shikimate. Sunflower XRQ genome contains three gene sequences that are predicted to encode EPSP synthases (Ha4g0122731, Ha15g0497011, and Ha16g0520001) (Badouin *et al.*, 2017) but their subcellular localization is currently unknown and no chloroplastic transit peptide can be identified with certainty in any of them.

Since several intermediates of chlorogenate synthesis seem to be affected simultaneously by CO<sub>2</sub>/O<sub>2</sub> conditions (phenylalanine, quinate, and caffeate), it is possible that several steps of the shikimate pathway are metabolic control points at the origin of the pattern seen here. 3-deoxy-D-arabino heptulosonate-7-phosphate synthase (DAHPS) is the first step of the pathway, and has been shown to be redox controlled via thioredoxins (Entus *et al.*, 2002). Also, 3-dehydroquinase is a NAD<sup>+</sup>-dependent enzyme and thus could depend on chloroplastic free NAD<sup>+</sup> concentration (although NADH represents only a few % of total chloroplastic NAD including in the light, Heber & Santarius, 1965).

Taken as a whole, our results show there is a regulation of the flux through the shikimate pathway by CO<sub>2</sub> and O<sub>2</sub> conditions. This may involve photorespiration-driven changes in PEP availability, remobilization and post-translational regulation by redox conditions, but further work is required to clarify this aspect.

Downstream metabolism is affected by both CO<sub>2</sub> and O<sub>2</sub>, causing changes in photosynthetic yield of net N assimilation

One of the most visible effects of low oxygen was the increased biosynthesis of alanine, a biomarker of hypoxic conditions (for a review, see Limami *et al.*, 2014). Under our conditions, although inlet gas was at 0% O<sub>2</sub>, the atmosphere surrounding the leaf was not completely anoxic but at *c.* 0.03% O<sub>2</sub> simply because of O<sub>2</sub> evolution by photosynthesis. Our previous metabolomics analyses have shown that low gaseous oxygen triggered a hypoxic response in illuminated leaves, with a reorchestration of nitrogen and sulphur metabolism (Abadie *et al.*, 2017a). Here, absolute quantitation using <sup>13</sup>C-labelling showed that alanine accumulation under 0% O<sub>2</sub> was considerable, of *c.* 0.3 μmol m<sup>-2</sup> s<sup>-1</sup>, that is, 1.4% of net photosynthesis. Importantly, alanine production utilizes pyruvate and thus its increase under hypoxia was at the expense of other pathways consuming PEP (such as chlorogenate synthesis) (Fig. 4) or pyruvate (TCAP and glutamate synthesis, Fig. 6).

Glutamate was also affected by gaseous conditions and represented more  $^{13}\text{C}$  (in  $\text{mmol m}^{-2}$ ) at high photosynthesis (21%  $380 \mu\text{mol mol}^{-1} \text{CO}_2$ , or 2%  $\text{O}_2$ ) compared to high photorespiration (low  $\text{CO}_2$  or 100%  $\text{O}_2$ ) (Fig. 6). However, when expressed in % of net photosynthesis, it represented more at high photorespiration, meaning that carbon allocation to glutamate increased. The stimulating effect of low  $\text{CO}_2$  on carbon allocation to glutamate and TCAP intermediates has been observed in several species (Gauthier *et al.*, 2010; Tcherkez *et al.*, 2012; Abadie *et al.*, 2017b). The present results show a concurrent effect of  $\text{CO}_2$  and  $\text{O}_2$  mole fraction, suggesting that glutamate synthesis regulation is influenced by both photorespiratory demand and carbon availability by photosynthesis. This would explain why at 2%  $\text{O}_2$ , carbon allocation to glutamate appeared similar to that under ‘usual’ conditions.

Fluxes calculated here were then used to compute the photosynthetic yield of net nitrogen assimilation (net N demand divided by net assimilation) (Fig. 7). Net nitrogen assimilation calculated here was the sum of glycine, serine, alanine and glutamate accumulation. It did not include chlorogenate since there is no net N requirement, phenylalanine being deaminated to form cinnamate (and then caffeate) (Maeda & Dudareva, 2012). While the N demand (in  $\mu\text{mol m}^{-2} \text{s}^{-1}$ ) is much higher at 0%  $\text{O}_2$  due to alanine accumulation, the yield is the highest at 100%  $\text{O}_2$ , meaning that high photorespiration triggers a relatively high need in N assimilation, here of *c.* 1.4% of net photosynthesis. Although the N demand calculated here is certainly underestimated (protein synthesis, and other amino acids are not accounted for) the order of magnitude is within  $0.05\text{--}0.3 \mu\text{mol m}^{-2} \text{s}^{-1}$  and matches values of N assimilation obtained using the assimilatory quotient (Rachmilevitch *et al.*, 2004). Our result clearly show that under ‘usual’ conditions, an important proportion of N demand is represented by the accumulation of photorespiratory intermediates glycine and serine. That is, photorespiratory metabolism is responsible for an excess need in N of *c.*  $2 \text{mmol N m}^{-2} \text{d}^{-1}$  which is substantial when compared to leaf N content (*c.*  $50 \text{mmol N m}^{-2}$ ). We nevertheless recognize that serine accumulation could have also been caused by metabolic pathways other than photorespiration, such as cytoplasmic phosphoserine synthesis (for a review, see Ros *et al.*, 2014). Because of the correlation between glycine and serine total content across the range of  $\text{CO}_2/\text{O}_2$  conditions, we suggest that the contribution of the cytoplasmic pathway was marginal under our conditions.

## Perspectives

The present study shows that most carbon fluxes in metabolism are not just proportional to net photosynthesis (C input). Further, it emphasizes interactions between carbon and nitrogen metabolism whereby the accumulation of photorespiratory intermediates leads to an extra-demand in nitrogen assimilation. Even though fluxes involved here look rather small at first glance ( $< 0.5 \mu\text{mol m}^{-2} \text{s}^{-1}$ ), the impact on N assimilation is evident, with an increased  $^{15}\text{N}$  (Gauthier *et al.*, 2010) and  $^{13}\text{C}$  allocation (here) to N assimilates as photorespiration increases. In fact, leaf N assimilation requirement doubles at high photorespiration compared to 'usual' conditions (Fig. 7). Nitrogen assimilation is not the sole pathway to be influenced by  $\text{CO}_2$  and  $\text{O}_2$  mole fraction: we show here changes in both sucrose and secondary metabolism, thereby altering the requirement in nucleotides (typically, UTP required for sucrose synthesis, and ATP for chlorogenate synthesis) and PEP. We anticipate all of these metabolic changes to have potentially two significant consequences for plant carbon balance: First, the day respiration rate (non-photorespiratory  $\text{CO}_2$  evolution in the light) should vary concurrently with  $\text{CO}_2$  and  $\text{O}_2$  mole fraction (for a review, see Tcherkez *et al.*, 2017). Second, if the accumulation of photorespiratory intermediates is not compensated for by a lower triose phosphates utilization, this may impact on RuBP regeneration and cause a progressive decline in photosynthesis (Harley & Sharkey, 1991; Geiger & Servaites, 1994). The latter effect might be of importance under natural, transient conditions that promote photorespiration, such as low internal  $\text{CO}_2$  upon stomatal closure. We recognize that our study was conducted on sunflower, which accumulates metabolites such as chlorogenate (while other species may accumulate other secondary compounds, like glucosinolates in Brassicaceae, for example). But in principle, our results should be valid in other  $\text{C}_3$  species considering the similar influence of  $\text{CO}_2$  and  $\text{O}_2$  on glutamate biosynthesis in a range of species (Abadie *et al.*, 2017b). It is likely, however, that the impact of  $\text{CO}_2$  and  $\text{O}_2$  on N metabolism varies depending on nitrogen source and availability. For example, nitrate and ammonium based nutrition has been shown to have a differential effect on the  $\text{CO}_2$  compensation point and thus on the carboxylation-to-oxygenation ratio (Guo *et al.*, 2005). Similarly, sulphur availability is likely to influence the metabolic response to  $\text{CO}_2$  and  $\text{O}_2$  owing to the involvement of one-carbon metabolism in photorespiration. The impact of such nutrient conditions will be addressed in a subsequent study.

## Acknowledgements

We thank the Australian Research Council for its support via a Future Fellowship awarded to G.T., under contract FT140100645. We acknowledge the support of the NMR facility of the Research School of Chemistry (ANU) for providing free access to instruments. We thank Sophie Blanchet (University of Paris-Sud, France) for helping with perchloric extractions.

## Author contributions

C.A. undertook the experiments and NMR analysis. C.B. and C.A. performed LC-MS analyses. All authors discussed the results. G.T. wrote the paper.

## References

**Abadie C, Blanchet S, Carroll A, Tcherkez G. 2017a.** Metabolomics analysis of post-photosynthetic effects of gaseous O<sub>2</sub> on primary metabolism in illuminated leaves. *Functional Plant Biology* **44**: 929–940.

**Abadie C, Boex-Fontvieille ERA, Carroll AJ, Tcherkez G. 2016a.** In vivo stoichiometry of photorespiratory metabolism. *Nature Plants* **2**: 15220.

**Abadie C, Lothier J, Boex-Fontvieille E, Carroll AJ, Tcherkez G. 2017b.** Direct assessment of the metabolic origin of carbon atoms in glutamate from illuminated leaves using <sup>13</sup>C-NMR. *New Phytologist* **216**: 1079–1089.

**Abadie C, Mainguet S, Davanture M, Hodges M, Zivy M, Tcherkez G. 2016b.** Concerted changes in phosphoproteome and metabolome under different CO<sub>2</sub>/O<sub>2</sub> gaseous conditions in Arabidopsis rosettes. *Plant and Cell Physiology* **57**: 1544–1556.

**Albrizio R, Steduto P. 2003.** Photosynthesis, respiration and conservative carbon use efficiency of four field grown crops. *Agricultural and Forest Meteorology* **116**: 19–36.

**Atkins CA, Calvin DT. 1971.** Photosynthesis and CO<sub>2</sub> evolution by leaf discs: gas exchange, extraction, and ion-exchange fractionation of <sup>14</sup>C-labeled photosynthetic products. *Canadian Journal of Botany* **49**: 1225–1234.

**Aubert S, Gout E, Bligny R, Douce R. 1994.** Multiple effects of glycerol on plant cell metabolism. Phosphorus-31 nuclear magnetic resonance studies. *Journal of Biological Chemistry* **269**: 21420–21427.

**Badouin H, Gouzy J, Grassa CJ, Murat F, Staton SE, Cottret L, Lelandais-Brière C, Owens GL, Carrère S, Mayjonade B et al. 2017.** The sunflower genome provides insights into oil metabolism, flowering and Asterid evolution. *Nature* **546**: 148–152.

**Bloom A, Burger M, Kimball B, Pinter P. 2014.** Nitrate assimilation is inhibited by elevated CO<sub>2</sub> in field-grown wheat. *Nature Climate Change* **4**: 477–480.

**Bloom AJ, Smart DR, Nguyen DT, Searles PS. 2002.** Nitrogen assimilation and growth of wheat under elevated carbon dioxide. *Proceedings of the National Academy of Sciences, USA* **99**: 1730–1735.

**Boex-Fontvieille E, Davanture M, Jossier M, Zivy M, Hodges M, Tcherkez G. 2014.** Photosynthetic activity influences cellulose biosynthesis and phosphorylation of proteins involved therein in Arabidopsis leaves. *Journal of Experimental Botany* **65**: 4997–5010.

**Boex-Fontvieille E, Daventure M, Jossier M, Zivy M, Hodges M, Tcherkez G. 2013.** Photosynthetic control of Arabidopsis leaf cytoplasmic translation initiation by protein phosphorylation. *PLoS ONE* **8**: e70692.

**von Caemmerer S, Farquhar GD. 1981.** Some relationships between the biochemistry of photosynthesis and the gas exchange of leaves. *Planta* **153**: 376–387.

**Connor D, Sadras V. 1992.** Physiology of yield expression in sunflower. *Field Crops Research* **30**: 333–389.

**Dewar RC, Medlyn BE, McMurtrie RE. 1998.** A mechanistic analysis of light and carbon use efficiencies. *Plant, Cell & Environment* **21**: 573–588.

**Entus R, Poling M, Herrmann KM. 2002.** Redox regulation of Arabidopsis 3-Deoxy-d-arabino-Heptulosonate 7-Phosphate synthase. *Plant Physiology* **129**: 1866–1871.

**Foyer CH, Ferrario-Méry S, Huber SC. 2000.** Regulation of carbon fluxes in the cytosol: coordination of sucrose synthesis, nitrate reduction and organic acid and amino acid biosynthesis. In: Sharkey T, Govindjee, eds. *Photosynthesis: physiology and metabolism. Advances in photosynthesis and respiration, volume 9*. Dordrecht, the Netherlands: Springer, 177–203.

**Gauthier PPG, Bligny R, Gout E, Mahé A, Nogués S, Hodges M, Tcherkez GGB. 2010.** *In folio* isotopic tracing demonstrates that nitrogen assimilation into glutamate is mostly

independent from current CO<sub>2</sub> assimilation in illuminated leaves of *Brassica napus*. *New Phytologist* **185**: 988–999.

**Geigenberger P, Stitt M. 1991.** A “futile” cycle of sucrose synthesis and degradation is involved in regulating partitioning between sucrose, starch and respiration in cotyledons of germinating *Ricinus communis* L. seedlings when phloem transport is inhibited. *Planta* **185**: 81–90.

**Geiger DR. 1979.** Control of partitioning and export of carbon in leaves of higher plants. *Botanical Gazette* **140**: 241–248.

**Geiger DR, Servaites JC. 1994.** Diurnal regulation of photosynthetic carbon metabolism in C<sub>3</sub> plants. *Annual Review Plant Physiology Plant Molecular Biology* **45**: 235–256.

**Guo S, Schinner K, Sattelmacher B, Hansen U-P. 2005.** Different apparent CO<sub>2</sub> compensation points in nitrate- and ammonium-grown *Phaseolus vulgaris* and the relationship to non-photorespiratory CO<sub>2</sub> evolution. *Physiologia Plantarum* **123**: 288–301.

**Harley PC, Sharkey TD. 1991.** An improved model of C<sub>3</sub> photosynthesis at high CO<sub>2</sub>: reversed O<sub>2</sub> sensitivity explained by lack of glycerate reentry into the chloroplast. *Photosynthesis Research* **27**: 169–178.

**Heber U, Santarius KA. 1965.** Compartmentation and reduction of pyridine nucleotides in relation to photosynthesis. *Biochimica et Biophysica Acta* **109**: 390–408.

**Henkes S, Sonnewald U, Badur R, Flachmann R, Stitt M. 2001.** A small decrease of plastid transketolase activity in antisense tobacco transformants has dramatic effects on photosynthesis and phenylpropanoid metabolism. *The Plant Cell* **13**: 535–551.

**Hilbert DW, Reynolds JF. 1991.** A model allocating growth among leaf proteins, shoot structure, and root biomass to produce balanced activity. *Annals of Botany* **68**: 417–425.

**Hodges M, Dellerio Y, Keech O, Betti M, Raghavendra AS, Sage R, Zhu X-G, Allen DK, Weber APM. 2016.** Perspectives for a better understanding of the metabolic integration of photorespiration within a complex plant primary metabolism network. *Journal of Experimental Botany* **67**: 3015–3026.

**Huber SC. 1989.** Biochemical mechanism for regulation of sucrose accumulation in leaves during photosynthesis. *Plant Physiology* **91**: 656–662.

- Jacob J, Lawlor DW. 1992.** Dependence of photosynthesis of sunflower and maize leaves on phosphate supply, ribulose-1,5-bisphosphate carboxylase/oxygenase activity, and ribulose-1,5-bisphosphate pool size. *Plant Physiology* **98**: 801–807.
- Lal SK, Kelley PM, Elthon TF. 1994.** Purification and differential expression of enolase from maize. *Physiologia Plantarum* **91**: 587–592.
- Lehman RH, Rice EL. 1972.** Effect of deficiencies of nitrogen, potassium and sulfur on chlorogenic acids and scopolin in sunflower. *American Midland Naturalist* **87**: 71–80.
- Limami AM, Diab H, Lothier J. 2014.** Nitrogen metabolism in plants under low oxygen stress. *Planta* **239**: 531–541.
- Maeda H, Dudareva N. 2012.** The shikimate pathway and aromatic amino acid biosynthesis in plants. *Annual Review of Plant Biology* **63**: 73–105.
- Maleszewski S, Lewanty Z. 1972.** Effect of oxygen concentration on the incorporation of <sup>14</sup>C into products of photosynthesis in Balsam fir. *Zeitschrift für Pflanzenphysiologie* **67**: 305–310.
- Nakamura T, Osaki M, Shinano T, Tadano T. 1997.** Difference in system of current photosynthesized carbon distribution to carbon and nitrogen compounds between rice and soybean. *Soil Sci. Plant Nutr* **43**: 777–788.
- Penning De Vries FWT. 1983.** Modeling of growth and production. In: Lange OL, Nobel PS, Osmond CB, Ziegler H, eds. *Encyclopedia of plant physiology volume 12D. Physiological plant ecology*. Berlin, Germany: Springer, 117–150.
- Pick TR, Bräutigam A, Schulz MA, Obata T, Fernie AR, Weber APM. 2013.** PLGG1, a plastidic glycolate glycerate transporter, is required for photorespiration and defines a unique class of metabolite transporters. *Proceedings of the National Academy of Sciences, USA* **110**: 3185–90.
- Piques M, Schulze WX, Höhne M, Usadel B, Gibon Y, Rohwer J, Stitt M. 2009.** Ribosome and transcript copy numbers, polysome occupancy and enzyme dynamics in Arabidopsis. *Molecular Systems Biology* **5**: 314.
- Planchet E, Lothier J, Limami A. 2017.** Hypoxic respiratory metabolism in plants: reorchestration of nitrogen and carbon metabolisms. In: Tcherkez G, Ghashghaie J, eds. *Plant*

respiration: metabolic fluxes and carbon balance. Dordrecht, the Netherlands: Springer, 215–233.

**Rachmilevitch S, Cousins AB, Bloom AJ. 2004.** Nitrate assimilation in plant shoots depends on photorespiration. *Proceedings of the National Academy of Sciences, USA* **101**: 11506–11510.

**Rao IM, Terry N. 1995.** Leaf phosphate status, photosynthesis, and carbon partitioning in sugar beet (IV. Changes with time following increased supply of phosphate to low-phosphate plants). *Plant Physiology* **107**: 1313–1321.

**Ros R, Muñoz-Bertomeu J, Krueger S. 2014.** Serine in plants: biosynthesis, metabolism, and functions. *Trends in Plant Science* **19**: 564–569.

**Sage RF, Sharkey TD, Seemann JR. 1988.** The in-vivo response of the ribulose-1,5-bisphosphate carboxylase activation state and the pool sizes of photosynthetic metabolites to elevated CO<sub>2</sub> in *Phaseolus vulgaris* L. *Planta* **174**: 407–416.

**Servaites JC, Geiger DR. 1974.** Effects of light intensity and oxygen on photosynthesis and translocation in sugar beet. *Plant Physiology* **54**: 575–578.

**Sharkey TD, Berry JA, Raschke K. 1985.** Starch and sucrose synthesis in *Phaseolus vulgaris* as affected by light, CO<sub>2</sub>, and abscisic acid. *Plant Physiology* **77**: 617–620.

**Steck W. 1968.** Metabolism of cinnamic acid in plants: chlorogenic acid formation. *Phytochemistry* **7**: 1711–1717.

**Stitt M. 1990.** Fructose-2,6-bisphosphate as a regulatory molecule in plants. *Annual Review of Plant Physiology and Plant Molecular Biology* **41**: 153–185.

**Stitt M. 1991.** Rising CO<sub>2</sub> levels and their potential significance for carbon flow in photosynthetic cells. *Plant, Cell and Environment* **14**: 741–762.

**Strand A, Zrenner R, Trevanion S, Stitt M, Gustafsson P, Gardstrom P. 2000.** Decreased expression of two key enzymes in the sucrose biosynthesis pathway, cytosolic fructose-1,6-bisphosphatase and sucrose phosphate synthase, has remarkably different consequences for photosynthetic carbon metabolism in transgenic *Arabidopsis thaliana*. *The Plant Journal* **23**: 759–770.

**Sun J, Zhang J, Larue CT, Huber SC. 2011.** Decrease in leaf sucrose synthesis leads to increased leaf starch turnover and decreased RuBP regeneration-limited photosynthesis but not Rubisco-limited photosynthesis in Arabidopsis null mutants of SPSA1. *Plant, Cell & Environment* **34**: 592–604.

**Tcherkez G. 2013.** Is the recovery of (photo) respiratory CO<sub>2</sub> and intermediates minimal? *New Phytologist* **198**: 334–338.

**Tcherkez G, Bligny R, Gout E, Mahe A, Hodges M, Cornic G. 2008.** Respiratory metabolism of illuminated leaves depends on CO<sub>2</sub> and O<sub>2</sub> conditions. *Proceedings of the National Academy of Sciences, USA* **105**: 797–802.

**Tcherkez G, Gauthier P, Buckley TN, Busch FA, Barbour MM, Bruhn D, Heskell MA, Gong XY, Crous K, Griffin KL et al. 2017.** Leaf day respiration: low CO<sub>2</sub> flux but high significance for metabolism and carbon balance. *New Phytologist* **216**: 986–1001.

**Tcherkez G, Mahé A, Guérad F, Boex-Fontvieille ERA, Gout E, Lamothe M, Barbour MM, Bligny R. 2012.** Short-term effects of CO<sub>2</sub> and O<sub>2</sub> on citrate metabolism in illuminated leaves. *Plant, Cell & Environment* **35**: 2208–2220.

**Tohge T, Watanabe M, Hoefgen R, Fernie AR. 2013.** Shikimate and phenylalanine biosynthesis in the green lineage. *Frontiers in Plant Science* **4**: 62.

**Tzin V, Galili G. 2010.** The biosynthetic pathways for shikimate and aromatic amino acids in *Arabidopsis thaliana*. *The Arabidopsis book* **8**: e0132.

**Voll LM, Hajirezaei MR, Czogalla-Peter C, Lein W, Stitt M, Sonnewald U, Börnke F. 2009.** Antisense inhibition of enolase strongly limits the metabolism of aromatic amino acids, but has only minor effects on respiration in leaves of transgenic tobacco plants. *New Phytologist* **184**: 607–618.

**Walker BJ, South PF, Ort DR. 2016.** Physiological evidence for plasticity in glycolate/glycerate transport during photorespiration. *Photosynthesis Research* **129**: 93–103.

## Supporting Information

Additional Supporting Information may be found online in the Supporting Information tab for this article:

**Fig. S1** Chemical structure of chlorogenate.

**Fig. S2** Simplified biosynthetic pathway of chlorogenate.

**Fig. S3** Modelling used to compute build-up rates.

**Fig. S4** NMR identification of chlorogenate.

**Fig. S5** Isotopic pattern in chlorogenate.

**Fig. S6** Positional  $^{13}\text{C}$ -percentage in sucrose.

**Fig. S7** Relationship between expected and observed  $^{13}\text{C}$ -percentage.

**Fig. S8** Intramolecular  $^{13}\text{C}$  pattern in chlorogenate.

**Fig. S9**  $^{13}\text{C}$ -enrichment in phenylalanine and quinate.

**Fig. S10** NMR identification of glycerate.

**Fig. S11** Comparison of glycerate build-up rates.

**Fig. S12** Total carbon flux associated with metabolite build-up.

**Table S1** Summary of gaseous conditions used in this study

**Table S2** NMR chemical shifts of chlorogenate

Please note: Wiley Blackwell are not responsible for the content or functionality of any supporting information supplied by the authors. Any queries (other than missing material) should be directed to the *New Phytologist* Central Office.

## Figures

**Fig. 1** Major metabolic redistribution of fixed carbon in sunflower leaves. This figure shows (names in bold) metabolites that are most visible by  $^{13}\text{C}$ -NMR, that is, representing most significant  $^{13}\text{C}$  pools after  $^{13}\text{CO}_2$  labelling (NMR spectrum in Fig. 2). Metabolic pathways are highly simplified to facilitate reading. Chlorogenate biosynthesis is further described in Supporting Information Fig. S2. PEP, phospho*enol*pyruvate; RuBP, ribulose-1,5-bisphosphate; TP, triose phosphates

**Fig. 2**  $^{13}\text{C}$ -NMR spectra of sunflower leaf extracts, showing the signals of chlorogenate. Average spectra obtained without (blue) and with (red) labelling with  $^{13}\text{CO}_2$  at  $380\ \mu\text{mol mol}^{-1}\ \text{CO}_2$ , 21%  $\text{O}_2$ ,  $400\ \mu\text{mol m}^{-2}\ \text{s}^{-1}$  PAR and  $21^\circ\text{C}$  are shown on bottom. The spectral ratio ( $^{13}\text{C}$  enrichment spectrum) is shown on top (green). Peaks associated with chlorogenate (except for those of the sugar region) are indicated with black arrowheads. A full description of peaks associated with individual C-atom positions is given in Supporting Information Fig. S1. The region of COOH groups and sugars is simply indicated by a bracket. Note that the signal of maleate (internal standard) is sensitive to pH and thus has a slightly variable chemical shift, causing artificially a signal in the ratio (\*). The peak of fumarate is very high (elevated content of fumarate at natural abundance in leaves) but is not labelled (f). a, alanine C-3; b, non-labelled compound of the betaine family; s, serine C-2; g, glycine C-2 + malate C-3. Red arrowheads stand for C-atom positions in glutamate (C-2, 3 and 4 from left to right).

**Fig. 3**  $^{13}\text{C}$ -fixation and  $^{13}\text{C}$ -labelling pattern in sugars of sunflower leaves under different gaseous conditions. Net  $\text{CO}_2$  assimilation, in  $\mu\text{mol m}^{-2}\ \text{s}^{-1}$  (a);  $^{13}\text{C}$  amounts ( $\text{mmol m}^{-2}$ ) represented by net assimilated C, sugars, chlorogenate, other metabolites represented in NMR spectra, and starch + exported carbon (b), relationship between net assimilated  $^{13}\text{C}$  and  $^{13}\text{C}$  found in leaf sucrose (dark grey), glucose (light grey) and fructose (white), all in  $\text{mmol m}^{-2}$  (c);  $^{13}\text{C}$  percentage in sucrose (d), glucose (e) and fructose (f). In (b), note that  $^{13}\text{C}$ -amounts represented by chlorogenate and other compounds are small. The inset in (b) is a magnification of the  $^{13}\text{C}$ -amount in other compounds present in the leaf. In (c), continuous lines stand for proportionality linear regressions  $y = a.x$ ; slopes obtained therefrom are 0.39 (sucrose), 0.087 (glucose) and 0.044 (fructose). The dashed line stands for a hyperbolic regression. All regressions are significant ( $P < 0.05$ ). Letters stand for statistical classes (Anova,  $P < 0.05$ ) when gaseous conditions are compared. The x-axis shows  $\text{O}_2$  and  $\text{CO}_2$  conditions ( $\%-\mu\text{mol mol}^{-1}$ , respectively) ordered by increasing carboxylation-to-oxygenation ratio from left to right. A magnification of the  $^{13}\text{C}$ -content in chlorogenate is shown in Fig. 4. Values shown are mean $\pm$ SD.

**Fig. 4**  $^{13}\text{C}$ -labelling in chlorogenate and intermediates of chlorogenate synthesis of sunflower leaves. (a–c), analysis of  $^{13}\text{C}$ -content in chlorogenate by NMR:  $^{13}\text{C}$ -percentage in chlorogenate (a),  $^{13}\text{C}$  amount represented by leaf chlorogenate due to either chlorogenate at natural abundance (1.1%; coarse hatched) or labelled (fine hatched) (b), and relationship between total net assimilated  $^{13}\text{C}$  and  $^{13}\text{C}$  represented by labelled chlorogenate (c). (d)  $^{13}\text{C}$ -percentage in phenylalanine and quinate measured by LC-MS. In (b), note that no labelling in chlorogenate was found ( $\%^{13}\text{C}$  not larger than 1.1%) and thus there is only ‘natural’ chlorogenate (coarse hatched). In (c), the continuous line represents the 1% proportionality line (i.e.  $y = 0.01 x$ ). Letters stand for statistical classes (Anova,  $P < 0.05$ ) when gaseous conditions are compared (in (b), statistical classes refer to labelling  $^{13}\text{C}$  (fine hatched), not total  $^{13}\text{C}$ ). In (a), (b) and (d), the  $x$ -axis shows  $\text{O}_2$  and  $\text{CO}_2$  conditions ( $\%-\mu\text{mol mol}^{-1}$ , respectively) ordered by increasing carboxylation-to-oxygenation ratio from left to right. Values shown are mean $\pm$ SD.

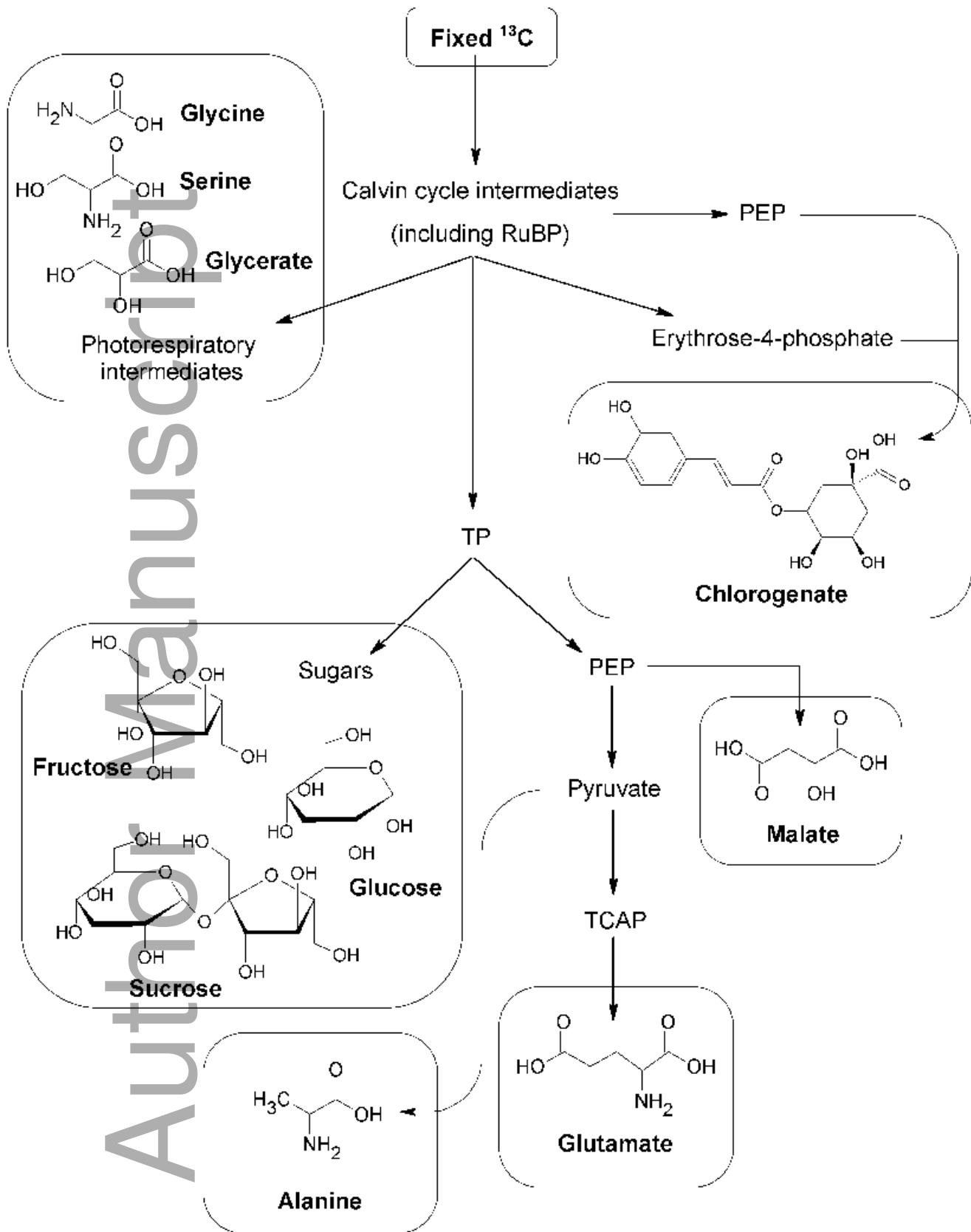
**Fig. 5**  $^{13}\text{C}$ -labelling pattern in glycerate, serine, glycine and alanine in sunflower leaves under different gaseous conditions.  $^{13}\text{C}$  amount (in  $\text{mmol }^{13}\text{C m}^{-2}$ ) allocated to these compounds during labelling (a), calculated build-up flux ( $\epsilon$  values in  $\mu\text{mol m}^{-2} \text{s}^{-1}$ , see the Materials and Methods section for calculation details) (b), and total leaf amount in glycine (light grey) and serine (dark grey) measured by LC-MS (c). The  $x$ -axis shows  $\text{O}_2$  and  $\text{CO}_2$  conditions ( $\%-\mu\text{mol mol}^{-1}$ , respectively) ordered by increasing carboxylation-to-oxygenation ratio from left to right. Values shown are mean $\pm$ SD.

**Fig. 6** Labelling pattern in malate and glutamate in sunflower leaves under different gaseous conditions.  $^{13}\text{C}$  amount (corrected for natural abundance) allocated to glutamate (calculated as 5/3 times the amount observed in C-2 + C-3 + C-4) and malate (calculated as 3 times the amount observed in C-2, so does not comprise the C-4 position) (a), apparent  $^{13}\text{C}$ -flux to glutamate (in  $\mu\text{mol }^{13}\text{C m}^{-2} \text{s}^{-1}$ ) and malate (in  $\mu\text{mol malate m}^{-2} \text{s}^{-1}$ ) synthesis (b) and glutamate and malate synthesis expressed as % of net assimilation: % C (glutamate) and % mol (malate) (c). Letters stand for statistical classes (Anova,  $P < 0.05$ ) when comparing gaseous conditions. The  $x$ -axis shows  $\text{O}_2$  and  $\text{CO}_2$  conditions ( $\%-\mu\text{mol mol}^{-1}$ , respectively) ordered by increasing carboxylation-to-oxygenation ratio from left to right. Values shown are mean $\pm$ SD.

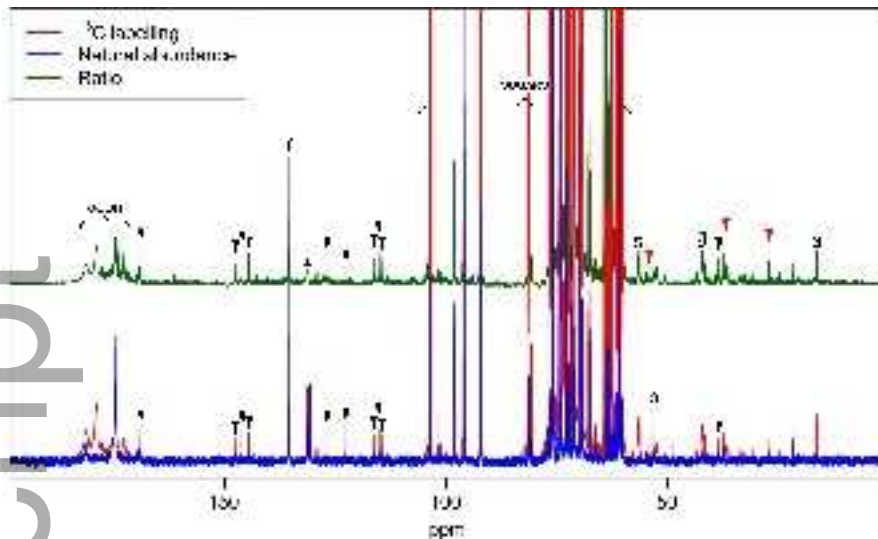
**Fig. 7** Net N demand driven by metabolite synthesis in sunflower leaves under different gaseous conditions. (a) Net nitrogen demand driven by synthesis of  $^{13}\text{C}$ -alanine,  $^{13}\text{C}$ -glutamate and accumulation of photorespiratory assimilates ( $\epsilon_{\text{Gly}} + \epsilon_{\text{Ser}}$ ) without (black) or with (white) remobilization of  $^{12}\text{C}$ -skeletons accounted for (assuming that glutamate and alanine neosynthesis is fed by 80% and 20% remobilized carbon, respectively). (b) Photosynthetic yield of net N assimilation, calculated as the ratio of net N demand (white bars in (a)) to net  $\text{CO}_2$  assimilation. Letters stand for statistical classes (Anova,  $P < 0.05$ ) when comparing conditions. The  $x$ -axis shows  $\text{O}_2$  and  $\text{CO}_2$  conditions ( $\%-\mu\text{mol}$

mol<sup>-1</sup>, respectively) ordered by increasing carboxylation-to-oxygenation ratio from left to right. Values shown are mean±SD.

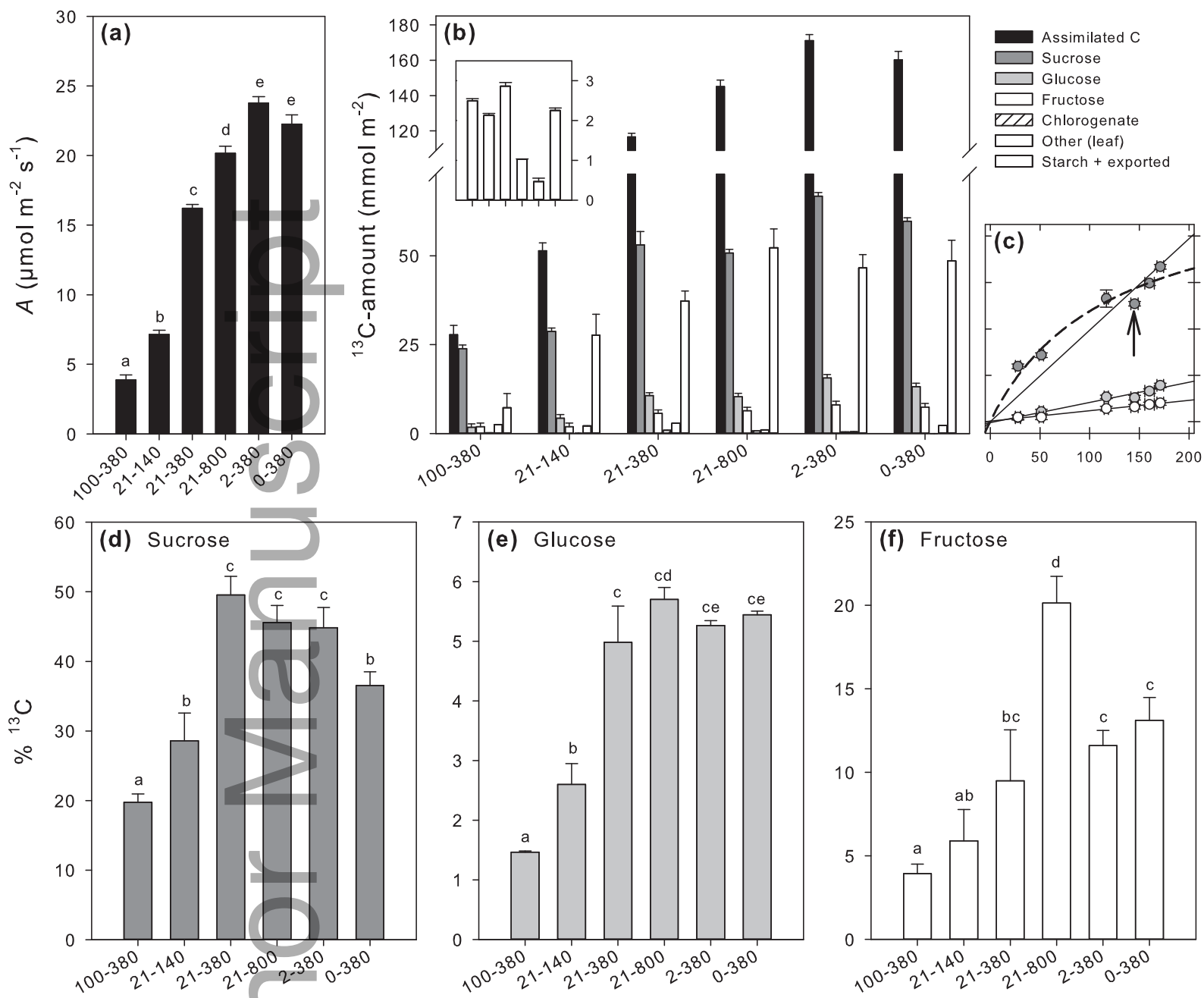
# Author Manuscript



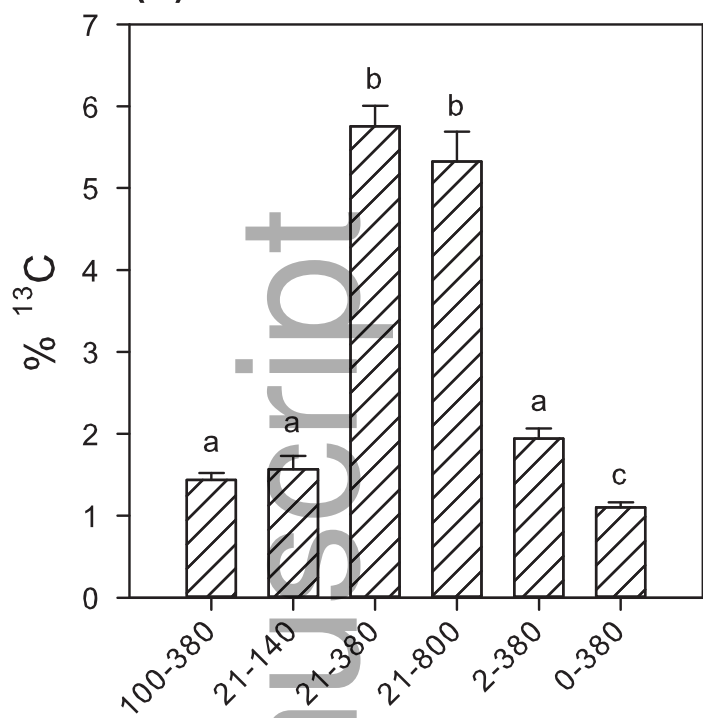
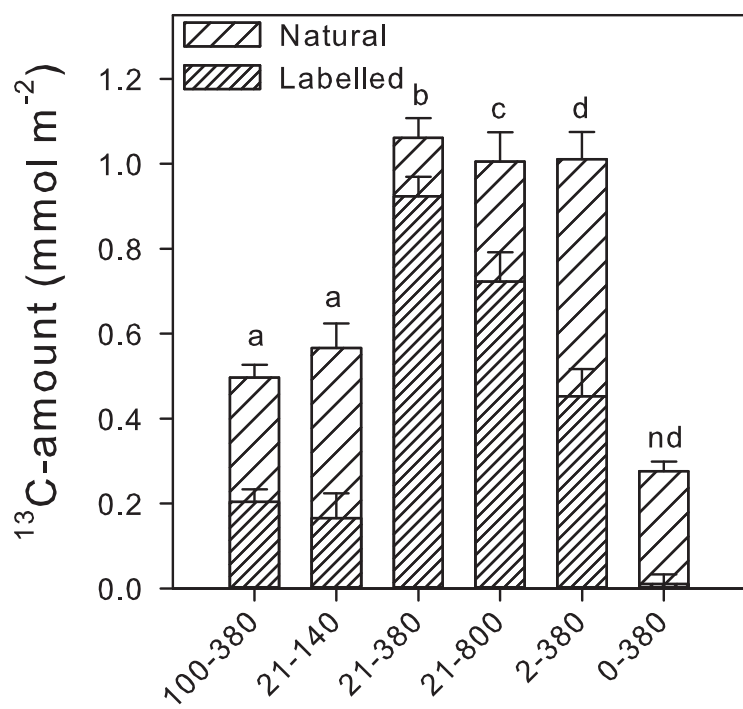
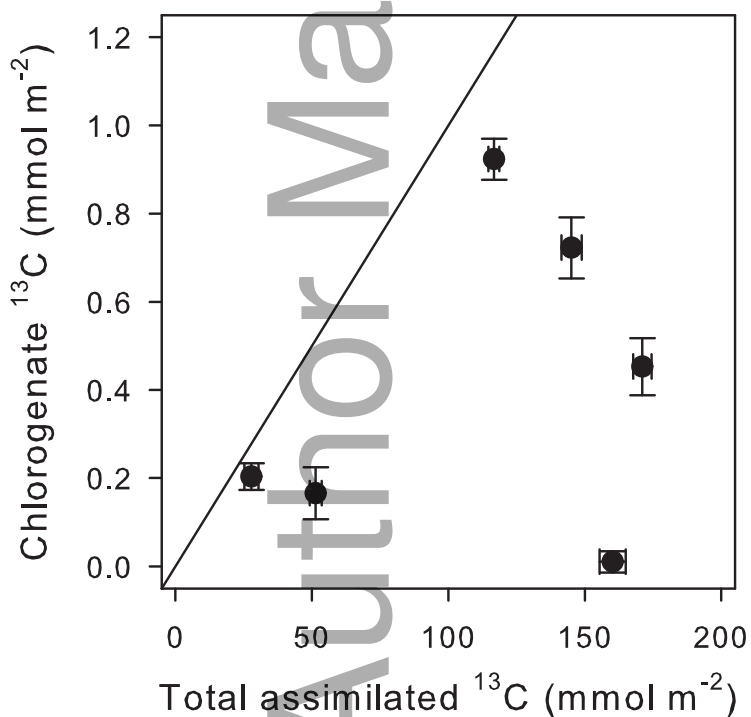
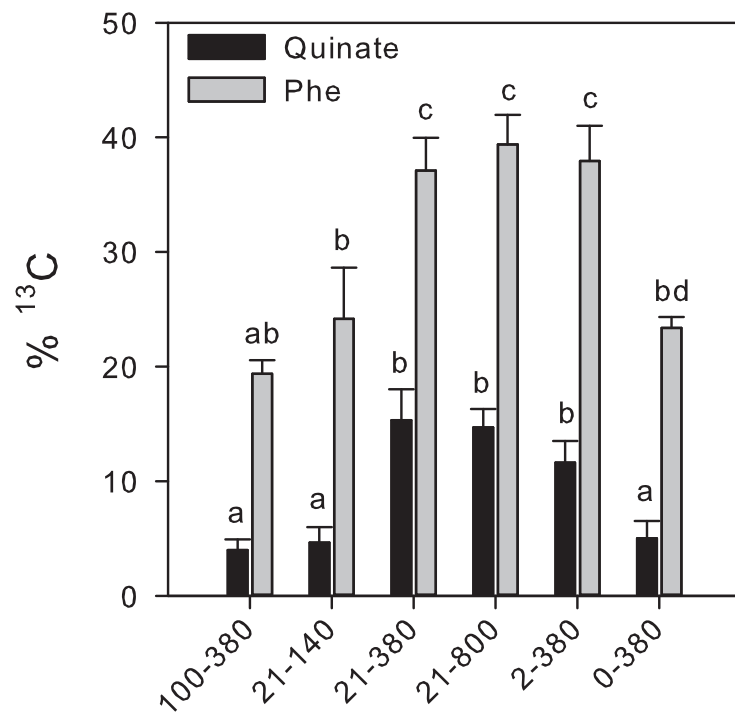
nph\_14984\_f1.tif



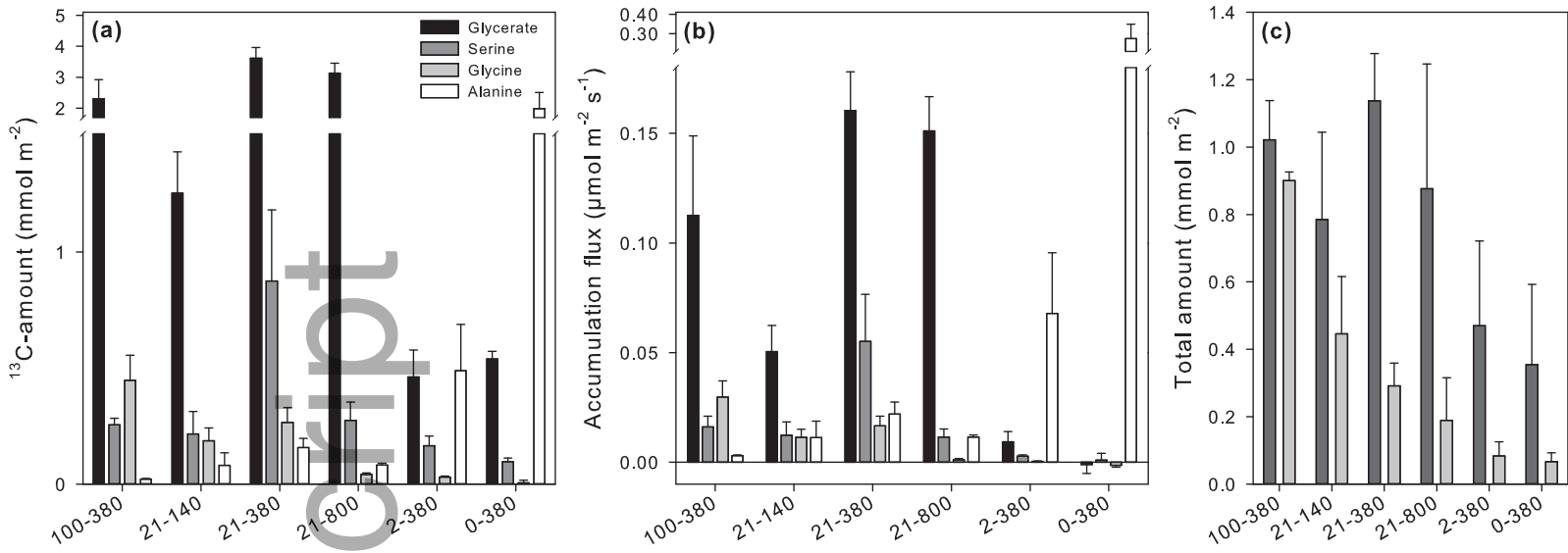
nph\_14984\_f2.tiff



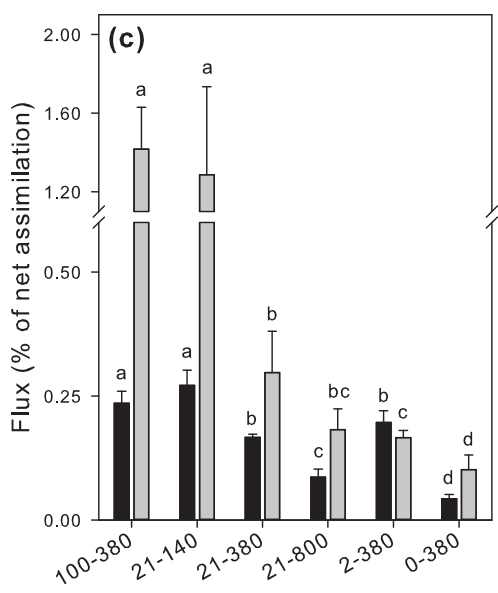
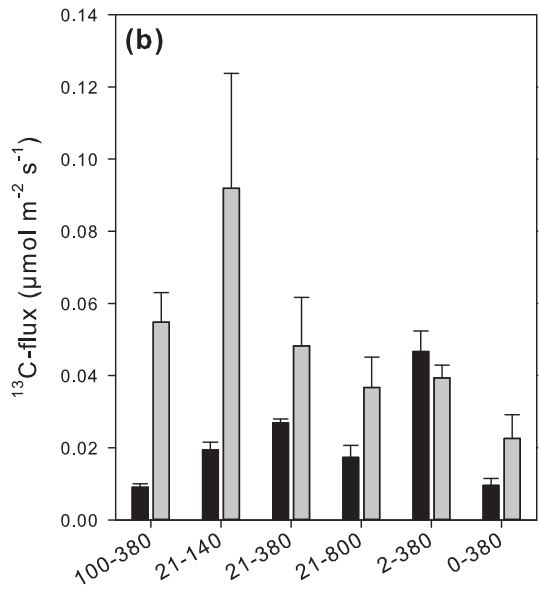
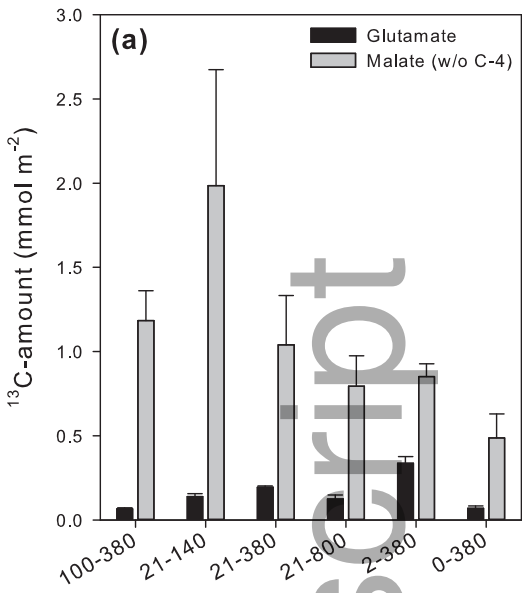
nph\_14984\_f3.eps

**(a)****(b)****(c)****(d)**

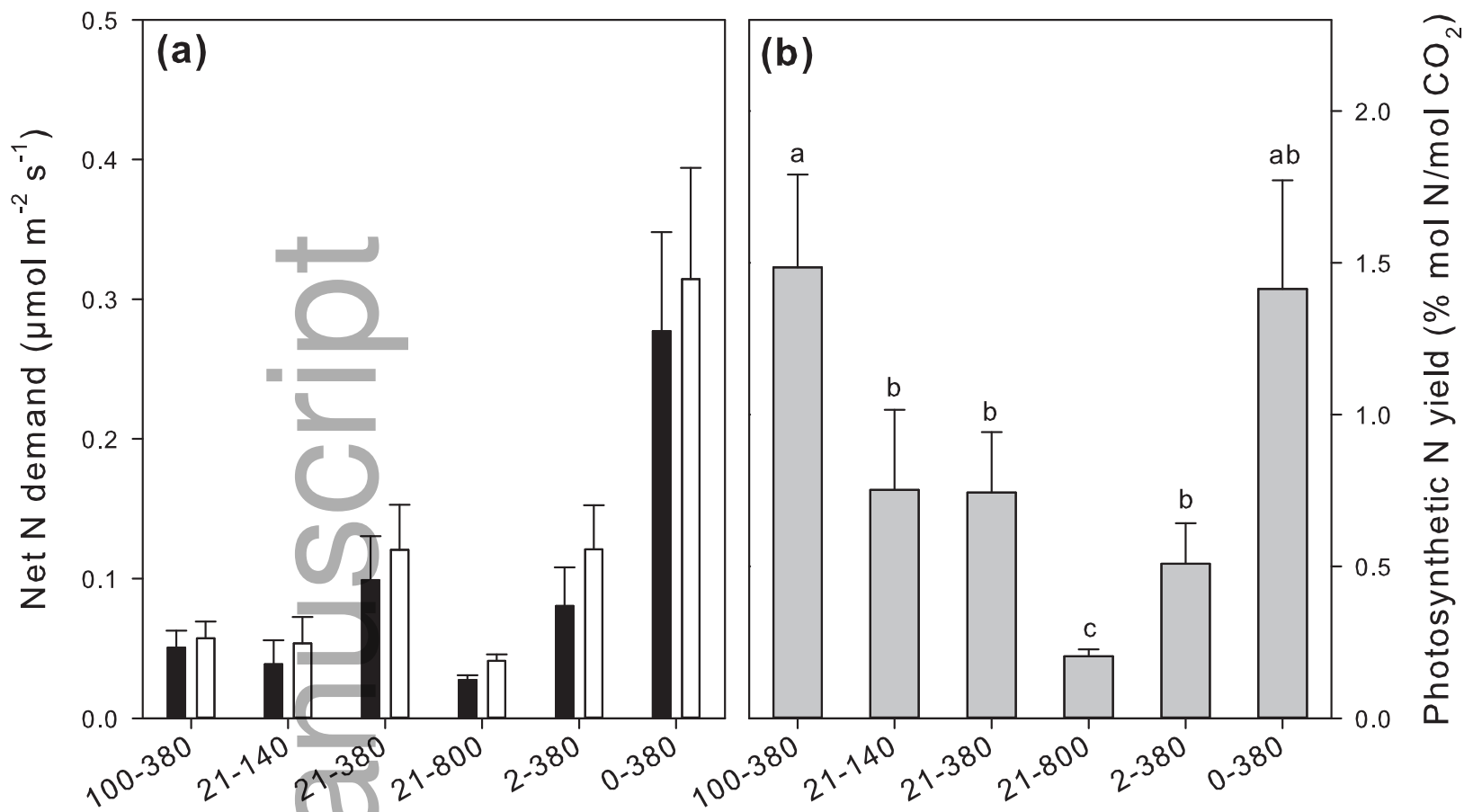
nph\_14984\_f4.eps



nph\_14984\_f5.eps



nph\_14984\_f6.eps



nph\_14984\_f7.eps